Transmission-Loss Performance of Additively Manufactured Hybrid Acoustic Liners for UAM Applications

K. Bakhet[a], B. Gaffney[b], B. Lee[a], E. McAleese[a], F. O'Connor[a,*], M. Sadlier[b]

[a] *MAI Mechanical and Manufacturing Engineering, Trinity College Dublin, Dublin, Ireland*
[b] *MAI Mechanical Engineering with Management, Trinity College Dublin, Dublin, Ireland*

Abstract

This paper experimentally assesses two compact, 3D-printed resonator liners designed for urban air mobility (UAM) ducts using the ASTM E2611 normal-incidence transfer-matrix method. A hybrid septa–Helmholtz concept (Group 6) and a variable-depth honeycomb concept (Group 8) were fabricated and tested in a 40×40 mm impedance tube across 500 Hz to 4 000 Hz. Transmission-loss (TL) spectra, band-averaged metrics, and peak attenuations were derived from repeated measurements and processed via data acquisition technologies. The hybrid liner delivered broadband attenuation with two pronounced peaks at 1.41 kHz and 2.51 kHz, outperforming the honeycomb design by an average of 7.7 dB across the band. We discuss the role of cavity coupling, manufacturing tolerances, and impedance matching in achieving target performance, and outline implications for UAM liner design where manufacturability and compactness are critical.

Keywords: Urban Air Mobility, Acoustic liners, Resonators, Transmission loss, Additive manufacturing

1. Introduction

Urban Air Mobility (UAM) is an emerging aviation sector focusing on electric vertical take-off and landing (eVTOL) aircraft that are anticipated to operate routinely over populous areas. According to NASA, typical UAM mission characteristics include vehicles that can travel up to 100 nautical miles, carry up to six passengers (or comparable cargo), and operate at heights of up to 3000 feet above the ground [1]. NASA has stated that "there will be noise issues that need to be addressed" because these operations would occur close to communities; therefore, NASA has formed an Urban Air Mobility Noise Working Group to identify gaps and recommendations pertaining to measurement and testing, human-response metrics, regulation and policy, and enabling tools and technologies [1]. The importance of mitigating transportation noise is reinforced by data associating noise exposure with sleep disruption. A systematic review and meta-analysis reports detrimental correlations between transportation noise and self-reported sleep outcomes, including increased odds of being highly sleep disturbed per 10 dB increase in nighttime noise level (L_{night}) for aircraft, road, and rail sources when survey questions explicitly referenced noise [2].

In this context, passive acoustic liners remain a practical mitigation strategy in aviation, with perforated liners widely utilised in aeroengines and related systems since the 1970s and often described as dissipating acoustic energy through thermoviscous and vortex-shedding mechanisms [3, 4]. This paper examines two resonator-based duct-liner ideas motivated by the need for compact attenuation of rotor-driven tonal and broadband noise components. Group 8 proposes a variable-depth honeycomb array of Helmholtz-type cavities tuned across approximately 1 000 Hz to 2 600 Hz to generate overlapping attenuation peaks [4], while Group 6 proposes a hybrid liner combining an extended-neck Helmholtz resonator chamber for improved low-frequency attenuation with a NASA Simplified Septa Acoustic Liner (SSAL)-inspired chamber intended to provide broadband mid-to-high frequency absorption [5].

Vehicle configuration has a significant impact on UAM aeroacoustics, influencing both the dominant noise mechanisms and the resulting frequency content. Many UAM concepts use multiple rotors for vertical lift in contrast to traditional rotorcraft. This adds complexity through varying rotational speeds, different operational states, and lower tip Mach numbers that can change the overall noise-generation profile. Interaction mechanisms such as blade–vortex interaction (BVI) and installation-related blade–airframe interaction (BAI), particularly when rotors operate in close proximity to airframe surfaces, can lead to more complex unsteady and potentially aperiodic loading-noise behaviour [1].

Normal-incidence transmission loss, TL_n, is frequently used to report performance to enable consistent comparison of liner concepts. In this method, the acoustic transfer matrix is derived from impedance-tube measurements by decomposing the recorded standing-wave field into forward- and backward-travelling waves, permitting extraction of TL_n and relating quantities such as α via the reflection

*Preprint submitted to *Trinity Research Methods Conference*. December 5, 2025
*Corresponding author: foconno1@tcd.ie

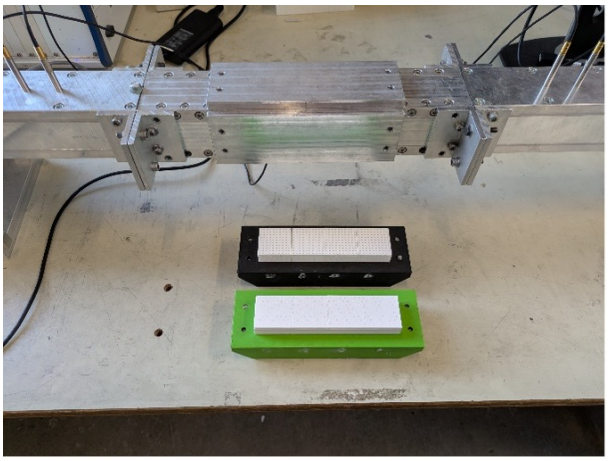

Figure 1: Printed samples and hard-wall reference insert [7].

Figure 2: Apparatus used for testing acoustic liners [7].

coefficient, R.

In the experimental campaign, a two-load transfer-matrix approach was executed in a 40×40 mm impedance tube with two microphones on each side of the specimen (four total), and sound transmission loss (STL) was reported over 500 Hz to 4 000 Hz for both Group 6 and Group 8 samples.

Since ASTM E2611 emphasises that observed transmission loss can rely heavily on specimen mounting and boundary conditions, the resulting STL/TL values are understood largely as controlled comparative data for the tested configuration [6, 7].

Accordingly, this paper explores and contrasts two student-designed resonator liner designs, namely Group 8's variable-depth honeycomb Helmholtz-cavity liner and Group 6's hybrid SSAL-inspired plus extended-neck Helmholtz liner [4, 5]. To provide a like-for-like assessment, performance is evaluated using the normal-incidence transfer-matrix methodology established in ASTM E2611-09, which reports TL_n (and associated quantities) under controlled mounting and boundary conditions [6].

2. Methodology

Samples

The acoustic liner specimens were 3D-printed with PLA on a Prusa Mini (FDM, 0.4 mm nozzle, adaptive layers). Edges were lightly dressed to ensure a gas-tight fit in the holder. Representative samples and the hard-wall insert are shown in Figure 1.

Impedance Tube and Instrumentation

Normal-incidence TL_n was measured in a 40×40 mm square tube using the ASTM E2611 two-load transfer-matrix method. as a The transmission loss was calculated as a function of the sound transmission coefficient, τ:

$$\mathrm{TL} = 10 \log_{10}\left(\frac{1}{\tau}\right), \tag{1}$$

Where relevant, the normal-incidence sound absorption coefficient, α, is also reported. This was used to calculate the reflection coefficient:

$$\alpha = 1 - |R|^2. \tag{2}$$

Four microphones (two per side) were acquired synchronously via an NI USB-4431. Broadband noise (≈20 Hz to 5 000 Hz) was used as the source. Rigid and anechoic terminations provided the two required loads; a GRAS calibrator set sensitivities. The setup is shown in Figure 2.

Procedure

For each design the specimen was inserted and sealed. Four-microphone pressures for both loads were recorded. The experiment was repeated three times. A hard-wall check (TL ≈0 dB) was performed to verify alignment, sealing, and calibration. Forward/backward waves were obtained from the four-microphone data and the transmission coefficient $\tau(f)$ was then used to compute TL via Equation (1).

Processing

Transfer-matrix inversion and TL calculation were implemented in MATLAB. For each sample, runs A–C were averaged. Band-averaged TL, peak magnitudes, and comparison plots were generated from the averaged spectra.

3. Optimisation Strategy

A variety of physical factors, such as resonant behaviour in cavities with varying depths and viscous losses in small chambers, affect the liner's acoustic performance. These mechanisms create a highly nonlinear relationship between the liner geometry and the resulting TL spectrum. Because of this, an optimisation strategy must handle nonlinear responses, operate without gradient information, and remain efficient despite the high computational cost of thermoviscous finite-element simulations. The Nelder–Mead simplex algorithm is suitable due to its robustness, derivative-free nature, and established use in the optimisation of acoustic metamaterials [8].

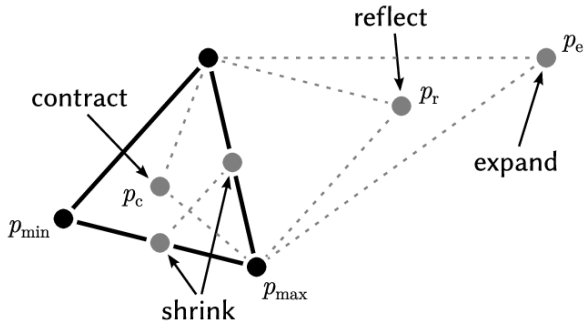

Figure 3: An iteration of the Nelder–Mead method over two-dimensional space [11].

Optimisation Objective and Design Parameters

The target may be to maximise broadband attenuation within a particular frequency range, tune peaks to align with tonal components, or suppress multiple harmonics related to the blade-pass frequency, depending on the UAM application. Corresponding design factors include cavity depths, internal cell dimensions, perforation diameter/distribution, face-sheet porosity/thickness, and any geometric parameters associated with holes in the resonant chambers [9].

Nelder–Mead Procedure

Nelder–Mead is a gradient-free direct-search method that requires only cost function evaluations. The algorithm constructs a simplex in parameter space and iteratively modifies its shape through reflection, expansion, contraction, and shrinkage operations, progressing toward improved performance. This process was visualised in Figure 3 by running an open-source MATLAB programme that was developed, and distributed under the MIT license [10].

Although inherently local and typically converging to a nearby optimum rather than a global one, it performs effectively when the number of design variables is moderate and each simulation is computationally expensive. Its suitability is supported by successful use in the design of acoustic metamaterials and resonant absorbers.

Required Input Data

At each iteration the acoustic performance of the geometry is evaluated using a thermoviscous acoustics finite-element model, which computes TL(f) or absorption coefficient $\alpha(f)$ across the band of interest. This modelling captures viscous boundary-layer effects, resonant cavity behaviour, and interactions between multiple degrees of freedom, representing the physical behaviour observed in impedance-tube measurements. Analytical expressions for Helmholtz-type resonance may be used to generate an informed initial guess, but the finite-element results form the primary input to the cost function.

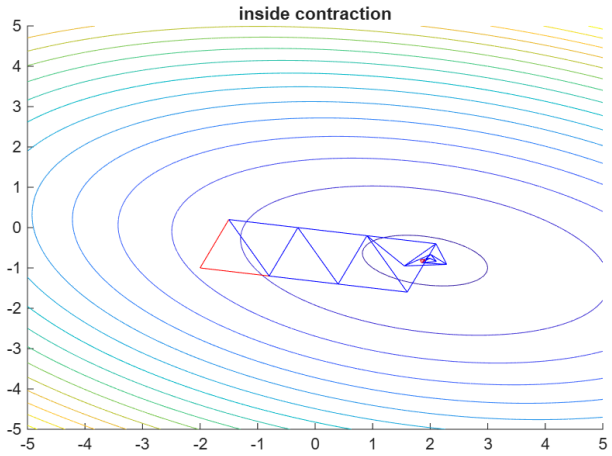

Figure 4: Nelder–Mead simplex iterations superimposed on the contour map of a two-dimensional cost function [10].

Cost Function Formulation

For broadband attenuation, the objective can be expressed as the negative average TL over the target band:

$$J = -\frac{1}{N}\sum_{i=1}^{N} \mathrm{TL}(f_i). \tag{3}$$

Penalties can be included for maximum allowable thickness, minimum printable features (FDM/MSLA), or acceptable pressure drop in ducted flow to maintain manufacturability and relevance to UAM applications [12].

Workflow

An initial simplex of n+1 candidate geometries (for n variables) is evaluated, and Nelder–Mead operations are applied until convergence thresholds are met. The resulting geometry is taken as the optimised solution for the defined noise-reduction objective [13].

4. Results of Manufactured Designs

The experimental testing used the ASTM E2611-09 two-load, four-microphone impedance-tube method to measure TL in the range 500 Hz to 4 000 Hz. Both manufactured liners—Group 6's hybrid septa–Helmholtz design and Group 8's variable-depth honeycomb design—were tested using the same sample across three identical tests to ensure measurement reliability. STL data were expressed in decibels and processed in MATLAB using the recorded transfer-matrix data. Peak values and frequency-specific metrics were taken from the averaged STL curves (mean average of Tests A-C) using an adapted MATLAB script (band-limited means and local maxima within specified windows). The band-averaged figures and comparison tables were then computed in Excel from the MATLAB-exported data and later plotted in MATLAB to ensure visual similarity. Reasoning is taken from the groups' research proposals and used solely to contextualise the presented results. All figures were exported at 600 dpi for publication-quality reproduction.

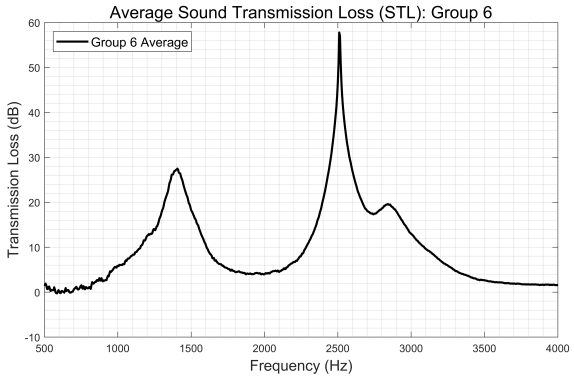

Figure 5: Average sound transmission loss (STL): Group 6 (Tests A–C).

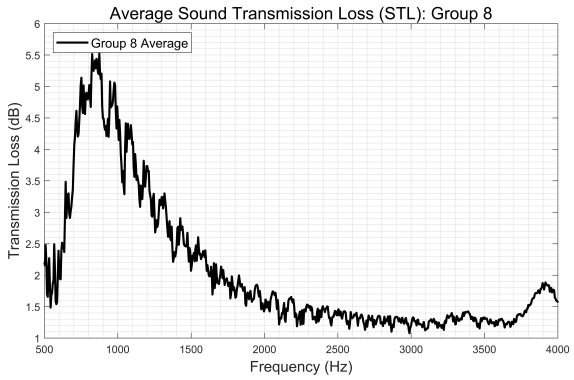

Figure 6: Average sound transmission loss (STL): Group 8 (Tests A–C).

Group 6: Hybrid Septa–Helmholtz Liner

Figure 5 shows the mean TL curve for Group 6, obtained by averaging Tests A–C. The attenuation band has two distinct resonant peaks: 27.50 dB at 1 406 Hz and a maximum of 57.79 dB at 2 510 Hz, indicating strong acoustic isolation. The minor fluctuations at lower frequencies (< 1 kHz) are attributed to standing-wave interference within the tube and were repeated across all three tests which confirms data reliability.

Group 8: Variable-Depth Honeycomb Liner

Figure 6 presents the averaged STL curve for Group 8. Compared to Group 6, the honeycomb liner exhibits substantially lower TL, with STL values below 6 dB across the entire range. A small resonant peak appears at 5.52 dB at 874 Hz and is followed by a gradual decay toward 4 kHz. The limited variation among the three tests demonstrates repeatable performance, but the low STL indicates weak resonant absorption in the structure.

Direct Comparison of Average Performance

Figure 7 overlays the averaged STL curves. Across 500 Hz to 4 000 Hz. Group 6 consistently provides higher TL: 9.75 dB on average versus 2.06 dB for Group 8. Group 8 is briefly higher from ∼500 Hz to 950 Hz as its variable-depth

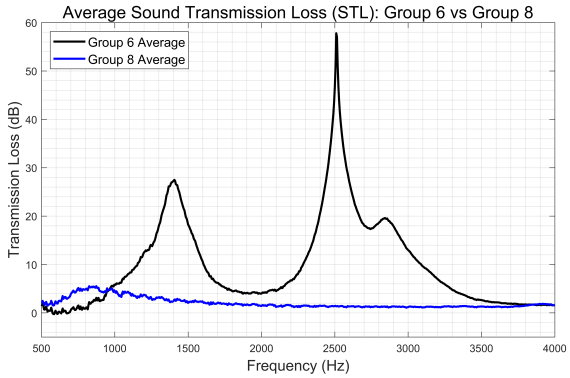

Figure 7: Overlay of average STL: Group 6 vs Group 8.

Table 1: Band-averaged STL (dB).

Design	0.5–1 kHz	1–2.5 kHz	2.5–4 kHz	0.5–4 kHz
Group 6	1.62	11.93	10.37	9.75
Group 8	3.83	2.19	1.34	2.06

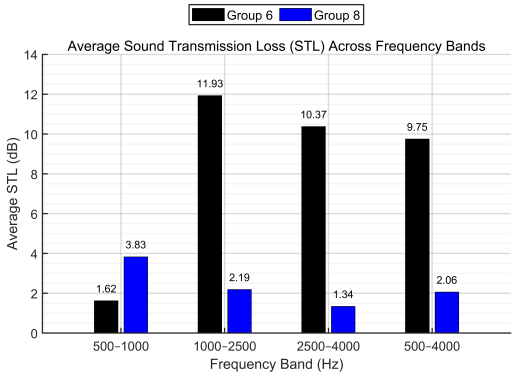

Figure 8: Average STL for Groups 6 and 8 across frequency bands.

honeycomb creates overlapping low-frequency Helmholtz-type resonances with thermoviscous wall losses that boost STL in that band. The largest separation occurs between 2 kHz to 3 kHz, where Group 6's Helmholtz-type cavities generate a strong resonance peak.

Band-Averaged Comparison

To quantify broadband behaviour, band averages (500 Hz to 1 000 Hz, 1 000 Hz to 2 500 Hz, 2 500 Hz to 4 000 Hz, and overall 500 Hz to 4 000 Hz) were calculated from the averaged STL data. The results, summarised in Table 1, highlight the stronger performance of Group 6 across three of the four bands. The mean STL difference across the full 500 Hz to 4 000 Hz range is 7.69 dB, confirming the superior broadband attenuation capability of Group 6's design.

5. Critique of the Performance of Designs

Group 6 Liner Performance

As outlined in their research proposal, Group 6 aimed to achieve broadband mid-to-high frequency absorption

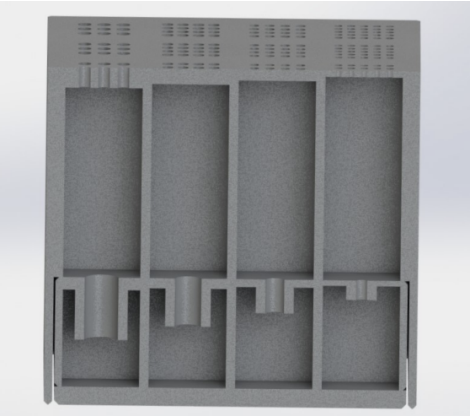

Figure 9: Group 6 liner CAD representation [5].

(400 Hz to 3 000 Hz) using a SSAL design from NASA, aided at low frequency (700 Hz to 1 000 Hz) by an extended-neck Helmholtz resonator [5, 12]. Goals included multiple resonance peaks and a broader absorption profile, with TL >5 dB up to 2 400 Hz. Their design achieved:

1. Two resonant peaks at 1 406 Hz and 2 510 Hz with STL 27.50 dB and 57.79 dB, respectively (Figure 5).
2. Sustained attenuation >5 dB from 1 kHz to 4 kHz (Figure 8).
3. Effective mid-to-high frequency absorption aligned with the target band.
4. An average STL of 9.75 dB over 500 Hz to 4 000 Hz.

The design underperformed in the 500 Hz to 1 000 Hz range, where average STL was only 1.6 dB, indicating limited low-frequency coupling. Despite this, results show that the Group 6 liner reduced noise significantly in the dominant audible rotor-noise spectrum without requiring excessively large geometries.

Group 8 Liner Performance

Group 8 adopted a honeycomb acoustic liner with varying cavity depths, acting as a series of Helmholtz resonators when combined [4]. The target was $\geq$10 dB attenuation over 1 kHz to 2.6 kHz, focusing on harmonics of the blade-passing frequency (BPF) [12]:

$$f_{\text{bp}} = \frac{n}{D\pi}\, v_r. \tag{4}$$

The prototype exhibited:

1. A peak STL of 5.52 dB at 874 Hz, followed by rapid decline.
2. An average STL <2.2 dB at >1 kHz.
3. An overall average STL of 2.06 dB from 500 Hz to 4 000 Hz.

Group 8 did not meet its attenuation targets. Minimal broadband overlap between target resonance peaks is evident in Figure 6. Evidence of impedance mismatch further reduced STL significantly [14]. The prototype behaved more like a standard duct than a functioning acoustic liner.

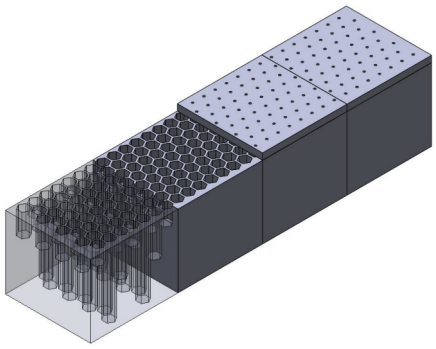

Figure 10: CAD model of Group 8's variable-depth honeycomb liner [4].

Comparison of Manufacturing Approaches

A direct comparison of STL responses demonstrates a significant divergence in performance across the same 500 Hz to 4 000 Hz band. When the averages are overlaid (Figure 7), Group 6 shows effective broadband attenuation; Group 8 shows a marginal, relatively flat response. Group 6 achieved peaks of 27.50 dB at 1 406 Hz and 57.79 dB at 2 510 Hz, consistent with multi-DOF coupling between septa and extended-neck Helmholtz chambers, yielding a broadband mean of 9.75 dB. Group 8 achieved only one low-magnitude resonance at 874 Hz at 5.52 dB, with STL consistently less than 6 dB elsewhere and a mean of 2.06 dB. The average difference is >7 dB in favour of Group 6, correlating to nearly five times less transmitted energy for the hybrid design. Band-averaged assessment (Figure 8) shows Group 6 leading in three of four bands, especially in the crucial 1 kHz to 2.5 kHz range.

Discrepancies are attributable to translation of design principles into prototypes. Group 6's spectrum features two high-Q resonances suggesting intended coupling and fidelity to design dimensions. Group 8's variable-depth honeycomb did not produce the multiple predicted resonances. FDM depth variation and surface roughness, with thin SLA face-sheet perforations, likely detuned resonances into a single subdued peak (Figure 6). Literature recognises the sensitivity of Helmholtz-type cavities to small geometric errors [12, 15].

When compared with prior liner concepts, Group 6 aligns with multi-resonator broadband liners (NASA SSAL-inspired) that leverage cavity coupling and overlapping attenuation bands [15]. In contrast, the Group 8 result is inconsistent with variable-depth honeycomb liners constructed with tight tolerance control [12].

Conclusions on Designs

Under the test conditions, Group 6 met its performance goals, producing meaningful peak attenuation and broadband response. Group 8, while repeatable, did not realise its intended multi-peaked behaviour, yielding limited broadband attenuation; the average STL difference between the two is 7.69 dB. This does not invalidate the graded-depth

concept; rather, it indicates sensitivity to geometric and perforation tolerances. The Group 6 hybrid liner operates as intended in this case, while the Group 8 honeycomb liner would require redesign and manufacturing re-evaluation to be fit for purpose.

CRediT Authorship Contribution Statement

K. Bakhet: Methodology, Resources, Writing–original draft. B. Gaffney: Methodology, Data curation, Writing–original draft. B. Lee: Formal analysis, Visualisation, Writing–original draft. E. McAleese: Conceptualisation, Resources, Writing–original draft. F. O'Connor: Supervision, Visualisation, Software, Project administration, Writing - Review & Editing. M. Sadlier: Software, Formal analysis, Data curation, Writing–original draft.

Acknowledgements

The authors thank the Trinity College Dublin School of Engineering—particularly Dr. Gareth J. Bennett and Dr. John Kennedy—for support during this module. We acknowledge peer input from Groups 6 and 8 during design reviews.

References

[1] S. A. Rizzi, D. L. Huff, Urban Air Mobility Noise: Current Practice, Gaps, and Recommendations, Tech. Rep. NASA/TP–2020-5007433, NASA Langley Research Center, Hampton, VA, USA, 2020. URL: https://ntrs.nasa.gov/citations/20205007433.

[2] M. Smith, M. Cordoza, M. Basner, Environmental noise and effects on sleep: An update to the who systematic review and meta-analysis, Environ. Health Perspect. 130 (2022) 076001. doi:10.1289/EHP10197.

[3] X. Liu, D. Zhao, D. Guan, S. Becker, D. Sun, X. Sun, Development and progress in aeroacoustic noise reduction on turbofan aeroengines, Prog. Aerosp. Sci. 130 (2022) 100796. doi:10.1016/j.paerosci.2021.100796.

[4] K. Oliver, S. Cleary, P. Luc, R. Pazar, A. Shortt, A. Evans, Research Proposal, Course report, Trinity College Dublin, University of Dublin, Dublin, Ireland, 2025. Group 08.

[5] B. Arnaud, P. Hickey, C. Hutchinson, R. Leask, S. McDermott, M. Runham, Hybrid Acoustic Liner Design for Urban Air Mobility Noise Reduction, Course report, Trinity College Dublin, University of Dublin, Dublin, Ireland, 2025. Group 06.

[6] Standard test method for measurement of normal incidence sound transmission of acoustical materials based on the transfer matrix method, 2009. URL: https://standards.iteh.ai/catalog/standards/astm/d63a9d30-3b6e-4cd5-886a-40dada3d8f33/astm-e2611-09.

[7] J. Kennedy, Test Report—Research Methods 2025/26, Test Rep., Trinity College Dublin, School of Engineering, Dublin, Ireland, 2025. Nov. 2025.

[8] J. Wang, H. Zhou, Optimization of low frequency acoustic absorption characteristics of underwater acoustic cover based on nelder–mead simplex method, J. Phys.: Conf. Ser. 2095 (2021) 012082. doi:10.1088/1742-6596/2095/1/012082.

[9] O. Ogun, J. Kennedy, Noise attenuation through optimised acoustic metamaterials: A low form factor design for targeted noise reduction, in: 2022 28th Int. Workshop on Thermal Investigations of ICs and Systems (THERMINIC), Dublin, Ireland, 2022, pp. 1–4. doi:10.1109/THERMINIC57263.2022.9950667.

[10] J. Borggaard, J. Burkardt, Nelder–mead optimization algorithm (MATLAB source code), https://people.sc.fsu.edu/~jburkardt/m_src/nelder_mead/nelder_mead.html, 2009. Accessed: 2025-12-05.

[11] J. Y. Cheng, T. Mailund, Ancestral population genomics using coalescence hidden Markov models and heuristic optimisation algorithms, Comput. Biol. Chem. 57 (2015) 80–92. doi:10.1016/j.compbiolchem.2015.02.001.

[12] M. B. Galles, D. M. Nark, M. G. Jones, E. Greenwood, Optimization of variable depth acoustic liners with grazing flow, in: AIAA SciTech 2024 Forum, Orlando, FL, USA, 2024. doi:10.2514/6.2024-2803, paper AIAA 2024-2803.

[13] M. A. Luersen, R. L. Riche, Globalized nelder–mead method for engineering optimization, Comput. Struct. 82 (2004) 2251–2260. doi:10.1016/j.compstruc.2004.03.072.

[14] F. Wu, Z. Ju, Z. Geng, J. Zhao, M. Hu, G. She, H. Pu, J. Luo, P. Xiang, Low frequency and broadband sound attenuation by meta-liner under grazing flow and high sound intensity, AIP Adv. 12 (2022) 085109. doi:10.1063/5.0102198.

[15] B. M. Howerton, J. R. Kreitzman, C. Solano, Extending acoustic liner bandwidth with simple embedded septa, in: 30th AIAA/CEAS Aeroacoustics Conf., Rome, Italy, 2024. doi:10.2514/6.2024-3302, paper AIAA 2024-3302.